Time-Optimal Path Parameterization for Critically Dynamic Motions of Humanoid Robots

Quang-Cuong Pham and Yoshihiko Nakamura
Department of Mechano-Informatics
University of Tokyo, Japan

***Abstract*—Planning collision-free, dynamically-balanced movements for humanoid robots is a challenging problem. An effective approach consists of first planning a motion satisfying geometric and kinematic constraints (such as collision avoidance, joint angle limits, velocity limits, etc.) and, in a second stage, modifying this motion so that it respects dynamic balance criteria, such as those relative to the Zero Moment Point (ZMP). However, this approach currently suffers from the issue that the modified motion may give rise to new collisions with respect to the original motion, which can be very costly to deal with, especially for systems with many degrees of freedom and cluttered environments. Here we present an algorithm to modify the motions of humanoid robots under ZMP constraints without changing the original motion path, making thereby new collision checks unnecessary. We do so by adapting the minimum-time path parameterization under torque constraints algorithm of Bobrow et al. to the case of ZMP constraints. In contrast with a previous approach based on finite differences and iterative optimization to find the optimal path parameterization under ZMP constraints, our Bobrow-based algorithm finds this optimal parameterization in a single pass. We demonstrate the efficiency of this algorithm by simulations.**

I. Introduction

Planning collision-free, dynamically-balanced movements for humanoid robots is a challenging problem because of the robots' large numbers of degrees of freedom and the issue of balance inherently associated with the erect posture.

An effective approach consists of first generate robot motions that satisfy *geometric and kinematic* constraints, such as collision avoidance, joint angle limits, velocity limits, satisfaction of high-level tasks, etc. Many powerful and versatile algorithms (which can also be combined with each other) allow to do so, just to name a few: prioritized inverse kinematics with equality and inequality constraints (see e.g. [19, 5]), randomized motion planning (see e.g. [6, 20]), motion retargeting from captured data (see e.g. [3, 7]), etc.

To take into account the standing/walking balance issues, these approaches typically involve the further condition that the projection of the Center of Mass (CoM) on the ground stays within the convex hull of the ground contact points – which can indeed be expressed as a purely geometric constraint. However, this condition on the CoM effectively guarantees robot balance only when the robot is assumed to move *quasi-statically*, that is, with a close-to-zero speed. If the motion speed is non-negligible, the CoM condition is inoperative: there exist motions that satisfy the CoM condition without being dynamically balanced and, conversely, there exist motions that are dynamically balanced without satisfying the CoM condition. A much appropriate condition for *dynamic* balance is that the *Zero Moment Point* (ZMP) should stay in the convex hull of the ground contact points (cf. [17])

It is thus necessary, in a second step, to *modify* the motions computed by the previously mentioned algorithms to make them satisfy the condition for dynamic balance expressed by the ZMP. There are basically two methods to do so: the first method consists of scaling down the motion speed, such that the motion is executed in a quasi-static manner (cf. [6]). This method has the obvious drawback that it may generate very slow movements. The second method consists of "filtering" a non-dynamically-balanced motion into a dynamically-balanced one considering the whole-body dynamics (see e.g. the balance compensation algorithm [4] or the "dynamics filter" algorithm [18]). However, these algorithms suffer from a serious issue: they modify the motion *path*, such that the "filtered" motion may give rise to new collisions with respect to the original motion. Therefore, these algorithms must check collisions again at each time step, which can be very costly, especially when the robot has many degrees of freedom or when the environment is cluttered. In fact, it is well known that dealing with collisions in such cases takes the biggest part of the computation time during the kinematic planning step.

Here we modify the motion by *time-reparameterizing* it: the original motion path remains thus *unchanged*, making new collision checks unnecessary. In contrast with the "scaling down" method previously discussed, the motions retimed by this method are not necessarily quasi-static, and can indeed be sometimes even faster than the original motions. This method is based on an algorithm first developed by Bobrow and other researchers in the 80's and 90's, which allows efficiently finding a time-parameterization of a given motion path that minimizes the execution time while respecting actuator torque limits [1, 12, 13, 11] (from now on, we shall refer to this algorithm as the "Bobrow algorithm" for convenience, but in no way we are underestimating the essential contributions of the other researchers). The key of the present article is thus to express the ZMP constraints in a form compatible with the Bobrow algorithm. Fig. 1 summarizes our approach.

The idea of using path reparameterization to handle ZMP constraints has been previously proposed by Suleiman et

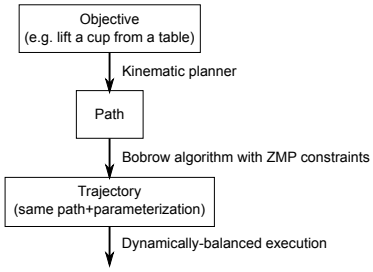

Fig. 1. Sketch of the "two-steps" approach.

al. [15]. While aware of the Bobrow algorithm, the authors thought it would be difficult to apply it to the case of humanoid robots. Instead, they followed an iterative optimization approach by considering a basis of the solution space (the space of the path parameterization functions s, cf. section II) and by optimizing the coefficients multiplying the basis functions. This approach thus usually yields a very large optimization problem: for instance, to obtain a satisfactory result in a whole-body reaching tasks, the authors needed to consider an optimization in 120 variables, which took 27 iterations to converge (and it was unclear whether the true optimum had been reached). Here we show that it is possible to apply the Bobrow algorithm to the case of humanoid robots and that, following this approach, the true optimal, *critical* (because the ZMP is always on the border of the authorized area, in contrast with [15] and in accordance with the theory of time-optimal control [1, 13]), path parameterization can be found *in a single pass*.

Note that, rather than following a "two-steps" approach as discussed so far, some methods take into account the ZMP constraint directly at the planning stage, by considering either a simplified inverted pendulum model of the robot (see e.g. [14] and references therein) or the robot whole-body dynamics (see e.g. [8] and references therein). While inverted-pendulum-based methods are appropriate to generate online walking motion, they are not suited for more complex behaviors involving for instance hierarchies of tasks. On the other hand, planning methods that take into account whole-body dynamics still lack the robustness and versatility of kinematics planning methods.

The rest of the article is organized as follows. In section II we show how to express the ZMP constraints in a form compatible with the Bobrow algorithm and discuss the specificities of these constraints. In section III, we show some simulation and experimental results on a humanoid robot. Finally, in section IV, we briefly discuss the advantages and limitations of the proposed approach, as well as its possible future developments.

II. Minimum-time path parameterization algorithm

A. Reducing the ZMP equations to the "Bobrow form"

Consider a legged robot composed of interconnected rigid links. A well-known condition for the robot dynamic balance is that the ZMP stays within the convex hull of the ground contact points at any time instant [17]. The X-coordinate of the ZMP is given by

$$x_{\mathbf{ZMP}} = \frac{\sum_i m_i(\ddot{z}_i + g)x_i - \sum_i m_i \ddot{x}_i z_i - \sum_i (\mathbf{M}_i)_y}{\sum_i m_i(\ddot{z}_i + g)},$$

where x_i, y_i, z_i are the coordinates of link i, $\boldsymbol{\omega}_i$ its angular velocity, m_i its mass, $\mathbf{I}_i$ its inertia matrix and $\mathbf{M}_i = \mathbf{I}_i\dot{\boldsymbol{\omega}}_i + \boldsymbol{\omega}_i \times \mathbf{I}_i\boldsymbol{\omega}_i$. The Y-coordinate of the ZMP can be computed by a similar formula [9].

Next, by forward kinematics, one can express $\mathbf{p}_i = (x_i, y_i, z_i)$ as a nonlinear function of the generalized coordinates $\mathbf{q}$ (typically, $\mathbf{q}$ may contain the translation and rotation of the base-link together with the joint angles)

$$\mathbf{p}_i = \mathbf{r}^p(\mathbf{q})$$

Successively differentiating the above relation yields (dropping the argument $\mathbf{q}$ for simplicity)

$$\dot{\mathbf{p}}_i = \mathbf{r}^p_{\mathbf{q}}\dot{\mathbf{q}} \tag{1}$$

and

$$\ddot{\mathbf{p}}_i = \mathbf{r}^p_{\mathbf{q}}\ddot{\mathbf{q}} + \dot{\mathbf{q}}^\top \mathbf{r}^p_{\mathbf{qq}}\dot{\mathbf{q}}, \tag{2}$$

where $\mathbf{r}^p_{\mathbf{q}}$ and $\mathbf{r}^p_{\mathbf{qq}}$ are respectively the Jacobian matrix (of dimension $3 \times n$, where n is the dimension of $\mathbf{q}$) and the Hessian tensor (of dimension $3 \times n \times n$) of $\mathbf{r}^p$ with respect to $\mathbf{q}$.

Assume that we are given a twice-differentiable motion trajectory $\mathbf{q}(t)_{t\in[0,T]}$. We say that s is a *path parameterization function* if it is an increasing, twice-differentiable function $s : [0, T'] \to [0, T]$. Next, $\mathbf{q}$ can be expressed as a function of the path parameter s as $\mathbf{q} = \mathbf{q}(s)$, which in turn yields

$$\dot{\mathbf{q}} = \mathbf{q}_s\dot{s} \tag{3}$$

and

$$\ddot{\mathbf{q}} = \mathbf{q}_s\ddot{s} + \mathbf{q}_{ss}\dot{s}^2 \tag{4}$$

Substituting (3) and (4) in (2) yields

$$\ddot{\mathbf{p}}_i = (\mathbf{r}^p_{\mathbf{q}}\mathbf{q}_s)\ddot{s} + (\mathbf{r}^p_{\mathbf{q}}\mathbf{q}_{ss} + \mathbf{q}_s^\top \mathbf{r}^p_{\mathbf{qq}}\mathbf{q}_s)\dot{s}^2$$

The above equation implies that $\ddot{x}_i$ can be expressed as a function of $s, \dot{s}^2, \ddot{s}$ as follows

$$\ddot{x}_i = a_{x_i}(s)\ddot{s} + b_{x_i}(s)\dot{s}^2,$$

and similarly, $\ddot{y}_i, \ddot{z}_i$ can be expressed as functions of $s, \dot{s}^2, \ddot{s}$.

Turning to the term in $\boldsymbol{\omega}_i$ in the expresion of $x_{\mathbf{ZMP}}$, remark that one can write

$$\boldsymbol{\omega}_i = \mathbf{r}^\omega(\mathbf{q})\dot{\mathbf{q}},$$

where $\mathbf{r}^\omega$ is a $3 \times n$ matrix. Thus, one has (dropping the argument $\mathbf{q}$ for simplicity)

$$\dot{\boldsymbol{\omega}}_i = \mathbf{r}^\omega\ddot{\mathbf{q}} + \dot{\mathbf{q}}^\top \mathbf{r}^\omega_{\mathbf{q}}\dot{\mathbf{q}},$$

where $\mathbf{r}^\omega_{\mathbf{q}}$ is the Jacobian tensor (of dimension $3 \times n \times n$) of

$\mathbf{r}^\omega$ with respect to $\mathbf{q}$. One can next write

$$\mathbf{M}_i = \mathbf{I}_i(\mathbf{r}^\omega \ddot{\mathbf{q}} + \dot{\mathbf{q}}^\top \mathbf{r}^\omega_{\mathbf{q}} \dot{\mathbf{q}}) + (\mathbf{r}^\omega \dot{\mathbf{q}}) \times \mathbf{I}_i \mathbf{r}^\omega \dot{\mathbf{q}}. \quad (5)$$

Substituting (3) and (4) in (5) yields

$$\mathbf{M}_i = (\mathbf{I}_i \mathbf{r}^\omega \mathbf{q}_s)\ddot{s} + [\mathbf{I}_i(\mathbf{r}^\omega \mathbf{q}_{ss} + \mathbf{q}_s^\top \mathbf{r}^\omega_{\mathbf{q}} \mathbf{q}_s) + (\mathbf{r}^\omega \mathbf{q}_s) \times \mathbf{I}_i(\mathbf{r}^\omega \mathbf{q}_s)]\dot{s}^2.$$

Thus $(\mathbf{M}_i)_x$ and $(\mathbf{M}_i)_y$ can also be expressed as functions of $s, \dot{s}^2, \ddot{s}$.

Recapitulating the previous calculations, one can express $x_{\mathbf{ZMP}}$ (and similarly $y_{\mathbf{ZMP}}$) as functions of $s, \dot{s}^2, \ddot{s}$ as follows

$$x_{\mathbf{ZMP}} = \frac{a(s)\ddot{s} + b(s)\dot{s}^2 + c(s)}{d(s)\ddot{s} + e(s)\dot{s}^2 + mg}, \quad (6)$$

where $m = \sum m_i$ is the total mass of the robot.

Remark It is actually not necessary to compute the full tensors $\mathbf{r}^p_{\mathbf{qq}}$ and $\mathbf{r}^\omega_{\mathbf{q}}$: it suffices indeed to evaluate the derivatives respectively of $\mathbf{r}^p_{\mathbf{q}}$ and of $\mathbf{r}^\omega$ along the direction given by $\mathbf{q}_s$. Similarly, the Jacobian matrices $\mathbf{r}^p_{\mathbf{q}}$ and $\mathbf{r}^\omega$ need only be evaluated in the directions of $\mathbf{q}_s$ and $\mathbf{q}_{ss}$.

In practice, the computation of the full $\mathbf{r}^p_{\mathbf{q}}$ and $\mathbf{q}_s$ can be performed extremely efficiently by robotics software : each evaluation took ∼0.2ms using OpenRAVE [2] on a personal computer. Each evaluation of $\mathbf{r}^p_{\mathbf{qq}}$ or $\mathbf{r}^\omega_{\mathbf{q}}$ in the direction of $\mathbf{q}_s$ thus also costs around 0.2ms.

B. Determining the minimum and maximum velocity curves

Assume for now that the convex hull of the ground contact points is a rectangle, such that the condition for balance is given by

$$\begin{cases} x_{\mathbf{min}} \leq x_{\mathbf{ZMP}} \leq x_{\mathbf{max}} \\ y_{\mathbf{min}} \leq y_{\mathbf{ZMP}} \leq y_{\mathbf{max}} \end{cases} \quad (7)$$

Using the previous development, the above conditions can be transformed into

$$x_{\mathbf{min}} \leq \frac{a(s)\ddot{s} + b(s)\dot{s}^2 + c(s)}{d(s)\ddot{s} + e(s)\dot{s}^2 + mg} \leq x_{\mathbf{max}},$$

and similarly for the Y-coordinate.

Note that the denominator is the vertical component of the ground reaction force, which is always strictly positive as long as the robot is not flying (see section II-D2). Thus the above equation is equivalent to

$$x_{\mathbf{min}}[d(s)\ddot{s} + e(s)\dot{s}^2 + mg] \leq a(s)\ddot{s} + b(s)\dot{s}^2 + c(s)$$

i.e.

$$x_{\mathbf{min}}[e(s)\dot{s}^2 + mg] - b(s)\dot{s}^2 - c(s) \leq [a(s) - x_{\mathbf{min}}d(s)]\ddot{s}$$

If $a(s) - x_{\mathbf{min}}d(s) > 0$, one has

$$\frac{[x_{\mathbf{min}}e(s) - b(s)]\dot{s}^2 + [x_{\mathbf{min}}mg - c(s)]}{a(s) - x_{\mathbf{min}}d(s)} \leq \ddot{s},$$

which can be rewritten

$$A\dot{s}^2 + B \leq \ddot{s}, \quad (8)$$

with $A = \frac{x_{\mathbf{min}}e(s) - b(s)}{a(s) - x_{\mathbf{min}}d(s)}$ and $B = \frac{x_{\mathbf{min}}mg - c(s)}{a(s) - x_{\mathbf{min}}d(s)}$.

If $a(s) - x_{\mathbf{min}}d(s) < 0$, inequality (8) is simply reversed. The case $a(s) - x_{\mathbf{min}}d(s) = 0$ corresponds to the more tricky "zero-inertia" case and should be dealt with specifically [11].

Similar inequalities involving $x_{\mathbf{max}}$, $y_{\mathbf{min}}$, $y_{\mathbf{max}}$ can be obtained following the same algebraic manipulations.

We thus have a certain number of inequalities $A^\alpha_j \dot{s}^2 + B^\alpha_j \leq \ddot{s}$, $j \in [1, n_\alpha]$ and $A^\beta_k \dot{s}^2 + B^\beta_k \geq \ddot{s}$, $k \in [1, n_\beta]$, with $n_\alpha + n_\beta = 4$.

For a given $(s, \dot{s})$, one can next compute the minimum and maximum admissible accelerations

$$\begin{cases} \ddot{s}^\alpha = \max_j A^\alpha_j \dot{s}^2 + B^\alpha_j \\ \ddot{s}^\beta = \min_k A^\beta_k \dot{s}^2 + B^\beta_k. \end{cases} \quad (9)$$

We now detail the computation of the minimum and maximum velocity curves. Consider $j \in [1, n_\alpha]$ and $k \in [1, n_\beta]$. There are three cases

- Case 1: $A^\alpha_j = A^\beta_k$. There are two subcases
  - if $B^\alpha_j \leq B^\beta_k$, then the couple (j, k) does not contribute to the maximum velocity or minimum velocity curve;
  - if $B^\alpha_j > B^\beta_k$, then there is no possible acceleration at any speed. The path is not dynamically feasible.
- Case 2: $A^\alpha_j < A^\beta_k$. Here the couple (j, k) may define a possible *lower bound* on $\dot{s}$. Let $r = \frac{B^\beta_k - B^\alpha_j}{A^\alpha_k - A^\beta_j}$. Again, there are two subcases
  - if $r < 0$, the couple (j, k) does not contribute to the maximum velocity or minimum velocity curve;
  - if $r \geq 0$, then $\gamma^-_{jk} = \sqrt{r}$ effectively defines a lower bound on $\dot{s}$.
- Case 3: $A^\alpha_j > A^\beta_k$. Here the couple (j, k) may define a possible *upper bound* on $\dot{s}$. Let $r = \frac{B^\beta_k - B^\alpha_j}{A^\alpha_k - A^\beta_j}$. Again, there are two subcases
  - if $r < 0$, then there is no possible acceleration at any speed. The path is not dynamically feasible;
  - if $r \geq 0$, then $\gamma^+_{jk} = \sqrt{r}$ effectively defines an upper bound on $\dot{s}$.

If one has not encountered a "non-dynamically feasible" case throughout the above calculations for all couples (j, k), one can then compute $\gamma^- = \max_{j,k} \gamma^-_{jk}$ and $\gamma^+ = \min_{j,k} \gamma^+_{jk}$, which define respectively the minimum and maximum velocity curves at s. Note that if, for some s, $\gamma^- > \gamma^+$, then the path is not dynamically feasible.

C. Integrating the optimal path parameterization in the $(s, \dot{s})$ plane

Equipped with the minimum and maximum admissible accelerations $[\ddot{s}^\alpha(s, \dot{s}),\ \ddot{s}^\beta(s, \dot{s})]$ and the minimum and maximum velocity curves (γ^-, γ^+), we are now ready to apply the Bobrow algorithm to find the minimum-time parameterization, which can be summarized as follows.

1) In the $(s, \dot{s})$ plane, start from $(s = 0, \dot{s} = \dot{s}_{\text{init}})$ and follow the vector field defined by the maximum admissible acceleration $\ddot{s}^\beta(s, \dot{s})$ until it hits either (a)

the maximum velocity curve, (b) the line $\dot{s} = 0$, (c) the minimum-velocity curve γ^- or (d) the line $s = s_{\text{end}}$. In cases (b) and (c) the movement is not dynamically feasible. In case (a), go to step 2. In case (d), go to step 3.

2) Search forward for the next switch point along the maximum velocity curve. A switch point is either a tangent point, a "zero-inertia" point or a discontinuity points. For more detail about how to find these points, cf. [13, 11]. From the switch point, go *backward* by following the vector field defined by the minimum admissible acceleration $\ddot{s}^{\alpha}(s, \dot{s})$ until it intersects the forward trajectory of step 1, and go *forward* following $\ddot{s}^{\beta}(s, \dot{s})$ – then continue as in step 1. The resulting forward trajectory will be the concatenation of the forward trajectory of step 1 until the intersection point, the backward trajectory from the intersection point to the switch point, and the forward trajectory from the switch point.

3) Start from $(s = s_{\text{end}}, \dot{s} = \dot{s}_{\text{end}})$ and go backward by following the vector field of $\ddot{s}^{\alpha}(s, \dot{s})$ until it intersects the forward trajectory of step 1 or 2. Then the resulting phase space trajectory will be the concatenation of the forward trajectory of step 1 or 2 until the intersection point and the backward trajectory of this step from the intersection point to s_{end}.

Finally, the so-obtained $(s, \dot{s})$ trajectory allows to compute $s(t)_{t\in[0,T']}$ by integration. For more implementation details about each step of the algorithm, the reader is referred to [1, 12, 13, 11]. An execution of the algorithm is illustrated in Fig. 3, bottom plot.

In practice, discretization is needed in the search for the switch points and the vector fields integration. Let N be the number of time samples in the discretization (in practice, it is sufficient to set $N = 100$ for a 1s motion). Then the construction of the maximum velocity curve and the switch point search is $O(nN)$ and the numerical integration is also $O(nN)$. Note that the discretization here is not of the same nature as the discretization for optimization in [15], which is associated with an exponential cost in the number of discrete optimization variables.

In some applications, a quasi-static motion is not dynamically balanced (consider e.g. a dynamic walking motion), yet it may be interesting to track the motion path *as slowly as possible*. In this case, one can run the same algorithm as presented above but by exchanging the role of $\ddot{s}^{\alpha}$ with that of $\ddot{s}^{\beta}$, and the role of γ^- with that of γ^+.

D. Some extensions

The previous development can be extended in the following directions.

1) Dealing with polygonal support areas: If the convex hull of the ground contact point is a polygon, then the system of inequalities (7) has a more general form

$$u_{1k}x_{\mathbf{ZMP}} + u_{2k}y_{\mathbf{ZMP}} + u_{3k} \leq 0, \quad k \in [1, K],$$

where K is the number of edges of the polygon. Such a system of inequalities can then be transformed into constraints upon $s, \dot{s}^2, \ddot{s}$ as in (8) following the same reasoning as earlier.

Theoretically, nonlinear support shapes can also be treated by the method but the calculations are more involved.

2) Other contact conditions: In addition to the ZMP constraints discussed so far, there are two other contact conditions that need to be checked in general. One condition is that the reaction force must be strictly positive – which we assumed without checking in section II-B. From equation (6), this can be expressed by

$$d(s)\ddot{s} + e(s)\dot{s}^2 + mg > 0,$$

which can be put in the form of equation (8) with $A = -e(s)/d(s)$ and $B = -mg/d(s)$.

Next, the condition of non-sliding around the Z-axis is given by

$$-\mu[d(s)\ddot{s} + e(s)\dot{s}^2 + mg] \leq \mathbf{T}_z \leq \mu[d(s)\ddot{s} + e(s)\dot{s}^2 + mg], \tag{10}$$

where μ is the coefficient of static friction and $\mathbf{T}_z = \sum_i m_i(y_i\ddot{x}_i - x_i\ddot{y}_i) - (\mathbf{M}_i)_z$ is the torque around the Z-axis. From the above expression of $\mathbf{T}_z$ and the development of section II-A, it is clear that $\mathbf{T}_z$ can also be expressed in terms of $s, \dot{s}^2, \ddot{s}$. Thus the inequalities (10) can also be put in the form of (8).

Note however that the conditions just mentioned are in practice more easily fulfilled than the ZMP conditions. We thus chose to leave them out in the simulations for the sake of clarity.

3) Taking into account velocity, acceleration and actuator torque limits: The ZMP constraints under the form of (8) can be combined with the existing velocity, acceleration and torque constraints (see also [10]). The complete algorithm thus allows to produce, in a single run, the minimum-time path parameterization respecting velocity, acceleration, torque limits *and* ZMP constraints.

4) Optimizing other criteria: It is also possible to consider other optimization criteria than the path traversal time. For instance, Verscheure et al. [16] reformulated the path-parameterization problem as a convex optimization problem (i.e. minimization of convex costs under linear equality and inequality constraints) and showed how to incorporate costs such as the thermal energy.

Since the ZMP constraints can be expressed as linear inequalities in $\dot{s}^2$ and $\ddot{s}$ [cf equation (8)], it should be straightforward to include these constraints into the framework of [16] (however note that doing so would make the approach similar to [15] in the sense that it woud rely on iterative optimization instead of a one-pass method). Within this framework, we could then consider costs related to the distance of the ZMP to the center of the support area, so as to maximize the balance. However, whether such costs can be expressed as convex functions of $\dot{s}^2$ and $\ddot{s}$ remains to be investigated.

III. Simulations

We tested this algorithm using a model of the HRP4 humanoid robot and the OpenRAVE simulation platform [2]. We considered a simple motion consisting of lifting a cup from a low table (see Fig. 2). The original and final postures were synthesized by inverse kinematics. Then the whole motion was computed by interpolating each degree of freedom of the robot by a third degree polynomial. Finally, the feet contact on the ground and collision avoidance were enforced by a simple kinematic filter.

This movement would be balanced if executed in a quasi-static manner: at each time instant, the projection of the CoM is contained within the area of the support area (cf. Fig. 3, green line). However, if the movement is executed at the planned speed (1.40s), the robot would fall because the ZMP trajectory would be outside the convex hull of the feet (Fig. 3, red line). We thus apply the algorithm described previously to find the minimum-time parameterization of the trajectory (1.39s) while respecting the ZMP constraints (see Fig. 2, bottom row and Fig. 3, blue line).

Note that at each time instant, at least one ZMP constraint is saturated (see Fig. 3, bottom plot). This *critical* behavior is indeed a necessary condition for time optimality [1, 13]. By contrast, the ZMP trajectories obtained in [15] almost never saturated their limits, indicating a possible sub-optimal behavior.

The computation time for the retiming algorithm was 4.7s on a 2GHz Intel Core Duo computer with 2GB RAM. To compare with the performance of other methods, note that

- Contrary to online motion planners (such as e.g. [5, 8]), which are concerned with the state and control input for the next time step, our algorithm computes the state and control input for the whole trajectory (here of duration 1.4s)
- Contrary to inverted-pendulum-based approaches (such as e.g. [14]), the optimization takes into account the dynamics of all body segments, and not only that of a low-dimensional model. Our approach can however be easily adapted to such models, which would yield a much lower computation time.
- The algorithm is currently prototyped in Python: we thus expect a significant gain in performance after transcription into C++.

IV. Discussion

We have presented an adaptation of the Bobrow algorithm to handle ZMP and other contact constraints. This allows finding very efficiently the minimum-time parameterization of a given motion path that respects such constraints associated with the standing/walking balance of humanoid robots. Combined with an upstream kinematic planner, our algorithm may therefore constitute a fast and versatile method to plan optimized, dynamically-balanced motions for humanoid robots (see Fig. 1).

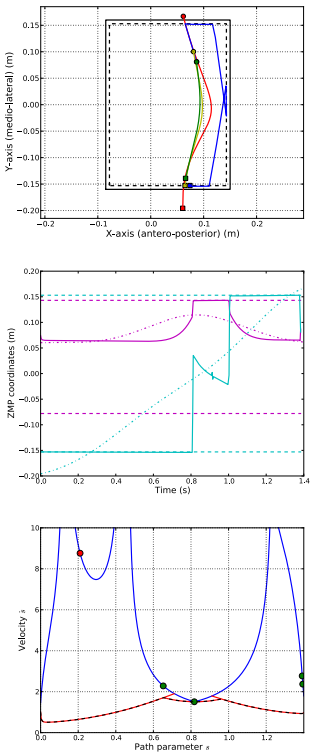

Fig. 3. **Top**: Trajectories of the ZMP and of the CoM projected on the ground. The black solid box shows the support area (the robot's left foot) and the black dashed box shows the conservative limits for balance. The trajectory of the projected CoM is in green. The beginnings and endings of the trajectory were marked respectively by squares and disks. The trajectory of the ZMP in the original motion (1.40s) is in red. Note that this trajectory is not contained within the support area: a robot executing this trajectory would thus stumble. The trajectory of the ZMP in the *retimed* motion (1.39s) is in blue. Note that the ZMP trajectory of the retimed motion (blue) is contained within the conservative limits ensuring thereby the balance. To achieve the same result, a "scaling down" method – where the velocity is uniformly reduced – would yield a much slower trajectory, of duration 2.90s (yellow). **Middle**: X- (magenta) and Y- (cyan) coordinates of the ZMP trajectories in time. Initial motion in dashed-dotted lines, retimed motion in plain lines, conservative limits in dashed lines. Note that at any time instant, at least one of the limits is saturated, which is a necessary condition for time optimality. **Bottom**: maximum velocity curve (blue) in the $(s, \dot{s})$ plane. The possible tangent points and "zero-inertia" points are marked in red and green respectively. The limiting curves are plotted in red and the final velocity curve is black dashed. For the definition of the terms just used and not defined here, cf. [13].

In addition to the extensions already discussed in section II-D, we are now considering the following theoretical and practical directions of development.

- Reactive, online motion planning;
- Discrete changes of the support areas as e.g. in walking;
- Integration of the algorithm with a complete kinematics planner and test on an actual humanoid robot.

Acknowledgments

We would like to thank Dr. R. Diankov for stimulating discussions and help with OpenRAVE. This work was supported by "Grants-in-Aid for Scientific Research" for JSPS fellows and by a JSPS postdoctoral fellowship.

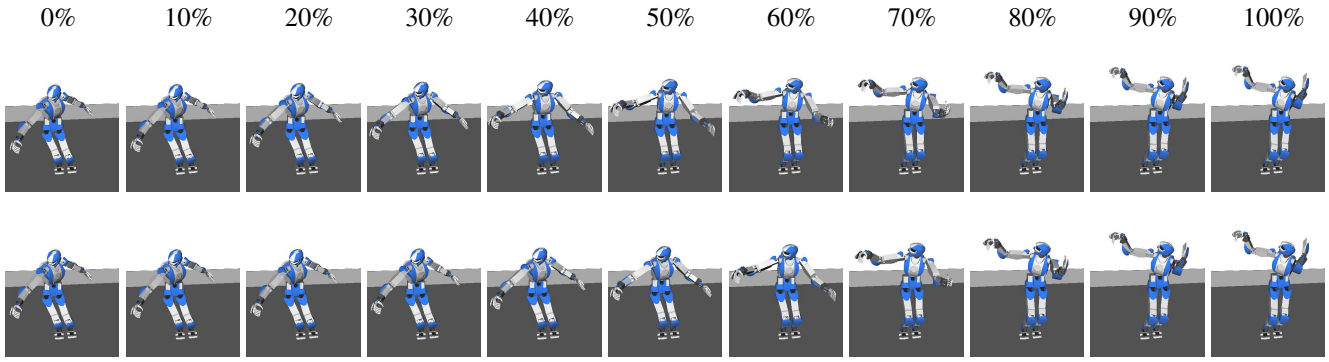

Fig. 2. Snapshots of the whole-body trajectories. **Top row**: original motion (1.40s). **Bottom row**: retimed motion (1.39s). Note that the differences between the two motions are very subtle, yet their balance properties are completely different.

REFERENCES

[1] J.E. Bobrow, S. Dubowsky, and JS Gibson. Time-optimal control of robotic manipulators along specified paths. *The International Journal of Robotics Research*, 4(3):3–17, 1985.

[2] R. Diankov. *Automated Construction of Robotic Manipulation Programs*. PhD thesis, Carnegie Mellon University, Robotics Institute, August 2010. URL http://www.programmingvision.com/rosen_diankov_thesis.pdf.

[3] M. Gleicher. Retargetting motion to new characters. In *ACM SIGGRAPH*, pages 33–42. ACM, 1998.

[4] Q. Huang, K. Tanie, and S. Sugano. Stability compensation of a mobile manipulator by manipulator motion: Feasibility and planning. *Advanced Robotics, 13*, 6(8): 25–40, 1999.

[5] O. Kanoun, F. Lamiraux, and P.-B. Wieber. Kinematic control of redundant manipulators: Generalizing the task-priority framework to inequality tasks. *IEEE Transactions on Robotics*, 27(4):785–792, 2011. doi: 10.1109/TRO.2011.2142450.

[6] J.J. Kuffner, S. Kagami, K. Nishiwaki, M. Inaba, and H. Inoue. Dynamically-stable motion planning for humanoid robots. *Autonomous Robots*, 12(1):105–118, 2002.

[7] J. Lee and S.Y. Shin. A hierarchical approach to interactive motion editing for human-like figures. In *ACM SIGGRAPH*, pages 39–48. ACM, 1999.

[8] N. Mansard. A dedicated solver for fast operational-space inverse dynamics. In *IEEE International Conference on Robotics and Automation*, 2012.

[9] P. Sardain and G. Bessonnet. Forces acting on a biped robot. center of pressure-zero moment point. *Systems, Man and Cybernetics, Part A: Systems and Humans, IEEE Transactions on*, 34(5):630–637, 2004.

[10] Z. Shiller and S. Dubowsky. On the optimal control of robotic manipulators with actuator and end-effector constraints. In *IEEE International Conference on Robotics and Automation*, volume 2, pages 614–620, 1985.

[11] Z. Shiller and H.H. Lu. Computation of path constrained time optimal motions with dynamic singularities. *Journal of dynamic systems, measurement, and control*, 114:34, 1992.

[12] K. Shin and N. McKay. Minimum-time control of robotic manipulators with geometric path constraints. *IEEE Transactions on Automatic Control*, 30(6):531–541, 1985.

[13] J.J.E. Slotine and H.S. Yang. Improving the efficiency of time-optimal path-following algorithms. *IEEE Transactions on Robotics and Automation*, 5(1):118–124, 1989.

[14] T. Sugihara, Y. Nakamura, and H. Inoue. Real-time humanoid motion generation through zmp manipulation based on inverted pendulum control. In *IEEE International Conference on Robotics and Automation*, pages 1404–1409, 2002.

[15] W. Suleiman, F. Kanehiro, E. Yoshida, J.P. Laumond, and A. Monin. Time parameterization of humanoid-robot paths. *IEEE Transactions on Robotics*, 26(3):458–468, 2010.

[16] D. Verscheure, B. Demeulenaere, J. Swevers, J. De Schutter, and M. Diehl. Time-optimal path tracking for robots: A convex optimization approach. *IEEE Transactions on Automatic Control*, 54(10): 2318–2327, 2009.

[17] M. Vukobratovic, B. Borovac, and D. Surdilovic. Zero-moment point–proper interpretation and new applications. In *Proceedings of the IEEE/RAS International Conference on Humanoid Robots*, volume 244, 2001.

[18] K. Yamane and Y. Nakamura. Dynamics filter – concept and implementation of online motion generator for human figures. *IEEE Transactions on Robotics and Automation*, 19(3):421–432, 2003.

[19] K. Yamane and Y. Nakamura. Natural motion animation through constraining and deconstraining at will. *IEEE Transactions on visualization and computer graphics*, pages 352–360, 2003.

[20] K. Yamane, J.J. Kuffner, and J.K. Hodgins. Synthesizing animations of human manipulation tasks. In *ACM Transactions on Graphics (TOG)*, volume 23, pages 532–539. ACM, 2004.